Numerical Simulation of Barium Sulfate Precipitation Process in a Continuous Stirred Tank with Multiple-Time-Scale Turbulent Mixer Model

Qinghua Zhang,[†] Zai-Sha Mao,[†] Chao Yang,*[,†,‡] and Chengjun Zhao[§]

Key Laboratory of Green Process and Engineering, Institute of Process Engineering, Chinese Academy of Sciences, Beijing 100190, China, Jiangsu Institute of Marine Resource Exploitation, Lianyungang 222005, China, and Shijiazhuang Chemical Fiber Corporation, Hebei 050032, China

Mixing of reagents is very important in precipitation processes, as it can significantly affect the size distribution and morphology of products. In this work, the influence of turbulent mixing on the course of barium sulfate precipitation process in a continuous stirred tank was investigated with multiple-time-scale turbulent mixer model. The effect of various operating conditions such as feed concentration, stirrer speed, and mean residence time on the barium sulfate precipitation process was clearly demonstrated. The simulation results were compared to the literature data, and good agreement is observed.

1. Introduction

Many chemical processes, such as the preparation of pharmaceutical, pigment, catalyst, and photographic material, water treatment, and offshore oil drilling, are involved with precipitation in one or more key operations. Because precipitation is a fast reaction process and very complex, the mixing at various scales plays a crucial role in determining the final crystal size distribution (CSD) and crystal morphology, which has attracted much attention.

The precipitation reaction of barium chloride and sodium sulfate as a model reaction has been widely investigated. Because many authors have studied such precipitation processes experimentally in detail,[1−3] theoretical prediction of the process is of key practical importance. In past years, different models have been proposed to describe the barium sulfate precipitation process, such as the interaction by exchange with mean model,[4,5] environment model,[6−8] and engulfment−deformation−diffusion model.[9,10]

CFD has become a powerful tool for the performance prediction, design, and scale-up of chemical reactors. This technique is particularly useful for studying mixing-controlled reactions. In recent years, some authors simulated numerically the precipitation process with CFD. The first report of successful CFD simulation of precipitation in a stirred tank was perhaps by Garside and Wei,[11] followed by Jaworski and Nienow.[12] They used CFD software to simulate the precipitation process in a stirred tank with the role of mixing at the molecular level (micromixing) completely neglected. However, the key role of micromixing in the precipitation process is generally recognized, which affects the rates of chemical reaction, nucleation, and crystal growth. It is therefore necessary to incorporate a suitable micromixing model into the model of a reactive precipitation process to accurately predict final product characteristics. For this reason, Piton et al.[13] and Marchisio et al.[14,15] utilized the finite-mode PDF (FM-PDF) model to describe the precipitation process in tubular and Talyor−Couette reactors, respectively. Wang et al.[16] also used the FM-PDF model to simulate the precipitation process of barium sulfate in a stirred tank. Vicum and Mazzotti,[17] Baldyga and Orciuch,[18,19] and Baldyga et al.[20] coupled CFD with the presumed-beta PDF and the multiple-time-scale turbulent mixer model on barium sulfate precipitation process in different operation modes and obtained good results. This multiple-time-scale turbulent mixer model considered all different mixing scales in the precipitation process, so it could capture correctly the whole system behavior. However, up to now there has been no report on the multiple-time-scale turbulent mixer model used in a continuous stirred tank.

In this work, the barium sulfate precipitation process in a continuous stirred tank was investigated by the multiple-time-scale turbulent mixer model. The effect of operating conditions, such as feed concentration, mean residence time, and stirrer speed, on the mean crystal size and crystal coeffecient of variation was studied numerically.

2. Precipitation Reactor

The cylindrical tank had a diameter of $T = 0.096$ m with a flat bottom and was filled with a solution up to $H = T$. The tank was equipped with four standard wall baffles of width $b = T/10$ and a flat blade turbine with diameter $D = T/3$ and the width of the agitator blades $W = 0.0096$ m[8]. The aqueous solutions of barium chloride and sodium sulfate were fed into the vessel through two pipes of diameter 0.008 m, which were located on its opposite sides at the bottom of the tank, midway between two baffles. The outlet pipe of diameter 0.008 m was located at the top and on one side of the vessel. The sketch of the stirred tank is shown in Figure 1.

3. Multiple-Time-Scale Turbulent Mixer Model

In turbulent flow, there are fluctuations of the particle velocity and concentrations of chemical species and crystalline particles. The averaged transport equation for the moment transformation of the population balance can be expressed as follows:[17]

$$\frac{\partial(\overline{u_{\mathrm{P}i}}\,\overline{m_j})}{\partial x_i} = \frac{\partial}{\partial x_i}\left(D_{\mathrm{PT}}\frac{\partial \overline{m_j}}{\partial x_i}\right) + 0^j\,\overline{R_{\mathrm{N}}} + j\,\overline{Gm_{j-1}} \qquad (1)$$

where D_{PT} is the local value of the particle turbulent diffusivity coefficient, $\overline{R_{\mathrm{N}}}$ is the local average nucleation rate, and $\bar{G}$ is the local average particle growth rate. Equation 1 should be solved together with the particle differential equations describing momentum, mass, and species balances. The local mean concentrations of barium and sulfate ions are given by

* To whom correspondence should be addressed. Tel.: +86-10-62554558. Fax: +86-10-62561822. E-mail: chaoyang@home.ipe.ac.cn.
[†] Chinese Academy of Sciences.
[‡] Jiangsu Institute of Marine Resource Exploitation.
[§] Shijiazhuang Chemical Fiber Corp.

10.1021/ie800722f CCC: $40.75
Published on Web 11/21/2008

$$\frac{\partial \overline{c_j}}{\partial t} + \frac{\partial(\overline{u_i}\,\overline{c_j})}{\partial x_i} = \frac{\partial}{\partial x_i}\left[(D_{\mathrm{m},j} + D_{\mathrm{T}})\frac{\partial \overline{c_j}}{\partial x_i}\right] - \frac{k_{\mathrm{a}}}{2}\frac{\rho_{\mathrm{BaSO_4}}}{M_{\mathrm{BaSO_4}}}\overline{Gm_2} \quad (2)$$

The most straightforward way to calculate the mean nucleation rate $\overline{R_{\mathrm{N}}}$ and $\overline{G_{mj}}$ is to consider them as the functions of average species concentrations $\overline{c_i}$. However, small-scale mixing effect is ignored in this way. For a better description, a multiple-time-scale turbulent mixer model[17] is used, in which the local instantaneous mole fraction of chemically and hydrodynamically passive tracer in the dimensionless form is defined as

$$f = \frac{c_{\mathrm{A}}^0}{c_{\mathrm{A0}}} \quad (3)$$

To compute the distributions of concentration variances of the mixture fraction, σ_s^2, the turbulent mixer model interprets the mixing process as three different contributions: σ_1^2, σ_2^2, and σ_3^2, which characterize the inertial-convective, viscous-convective, and viscous-diffusive mixing ranges, respectively, and can be described by the following spatial expression:

$$\sigma_s^2 = \overline{[f-\bar{f}]^2} = \sigma_1^2 + \sigma_2^2 + \sigma_3^3 \quad (4)$$

If the fluid were perfectly mixed, the concentration f would be equal to the average value $\bar{f}$, and the variance σ_s^2 would be equal to zero. The higher is the variance σ_s^2, the higher is the fluid segregation. The distribution of the average value of the mixture fraction $\bar{f}$ and the concentration variances σ_1^2, σ_2^2, and σ_3^2 are calculated by integrating the following expressions:

$$\frac{\partial \bar{f}}{\partial t} + \bar{u}_j\frac{\partial \bar{f}}{\partial x_j} = \frac{\partial}{\partial x_j}\left[(D_{\mathrm{m}} + D_{\mathrm{T}})\frac{\partial \bar{f}}{\partial x_j}\right] \quad (5)$$

$$\frac{\partial \sigma_i^2}{\partial t} + \bar{u}_i\frac{\partial \sigma_i^2}{\partial x_i} = \frac{\partial}{\partial x_i}\left[(D_{\mathrm{m},j} + D_{\mathrm{T}})\frac{\partial \sigma_i^2}{\partial x_i}\right] + R_{\mathrm{P}i} - R_{\mathrm{D}i}, \quad i = 1, 2, 3 \quad (6)$$

In eq 5, D_{m} is the molecular diffusivity and D_{T} is the turbulent diffusivity. $R_{\mathrm{P}i}$ and $R_{\mathrm{D}i}$ in eq 6 represent the production and dissipation terms:

$$R_{\mathrm{P1}} = 2D_{\mathrm{T}}\left(\frac{\mathrm{d}\bar{f}}{\mathrm{d}x_j}\right)^2 \quad (7)$$

$$R_{\mathrm{D1}} = R_{\mathrm{P2}} = \frac{\sigma_1^2}{\tau_{\mathrm{s}}} = \sigma_1^2 R\frac{\varepsilon}{k}, \quad R = 2 \quad (8)$$

$$R_{\mathrm{D2}} = R_{\mathrm{P3}} = E\sigma_2^2, E = 0.058\left(\frac{\varepsilon}{\nu}\right)^{1/2} \quad (9)$$

$$R_{\mathrm{D3}} = G\sigma_3^2, G = E\left(0.303 + \frac{17\,050}{S_{\mathrm{C}}}\right) \quad (10)$$

Having the values of $\bar{f}$ and σ_s^2, the probability density function of the passive tracer is expressed as the beta probability distribution of the mixture fraction of f:

$$\phi(x,f) = \frac{f^{v-1}(1-f)^{w-1}}{\int_0^1 y^{v-1}(1-y)^{w-1}\,\mathrm{d}y} \quad (11)$$

where

$$v = \bar{f}\left[\frac{\bar{f}(1-\bar{f})}{\sigma_s^2} - 1\right], \; w = \frac{v(1-\bar{f})}{\bar{f}}$$

The concentrations of barium and sulfate ions are calculated by an interpolation between the concentration $c_i^{\infty}(f)$ and $c_i^0(f)$ corresponding to an instantaneous and very slow precipitation. This method has been described by Baldyga and Orcruch[18,19] and Vicum and Mazzotti.[17] $c_i(f)$ is calculated by

$$c_i(f) = c_i^{\infty}(f) + \frac{\overline{c_i^{\infty}} - \overline{c_i^{\infty}}}{\overline{c_i^{\infty}} - \overline{c_i^{\infty}}}[c_i^0(f) - c_i^{\infty}(f)] \quad (12)$$

in which $c_i^0(f)$ can be calculated by

$$f = \frac{c_{\mathrm{A}}^0(f)}{c_{\mathrm{A0}}} = 1 - \frac{c_{\mathrm{B}}^0(f)}{c_{\mathrm{B0}}} \quad (13)$$

Also, the instantaneous precipitation concentration can be calculated from

$$f = \frac{c_{\mathrm{A}}^{\infty}(x,f) - c_{\mathrm{B}}^{\infty}(x,f) + c_{\mathrm{B0}}}{c_{\mathrm{A0}} + c_{\mathrm{B0}}} \quad (14)$$

Because reactants A and B cannot coexist in an instantaneous precipitation process, it is easy to determine the concentration of A, where $c_{\mathrm{A}}^{\infty}(f) > 0$, $c_{\mathrm{B}}^{\infty}(f) = 0$ or $c_{\mathrm{B}}^{\infty}(f) > 0$, $c_{\mathrm{A}}^{\infty}(f) = 0$. For the instantaneous precipitation, the average concentrations are given by

$$\overline{c_i^{\infty}} = \int_0^1 c_i^{\infty}(f)\phi(f)\,\mathrm{d}f \quad (15)$$

For the slow precipitation, $\overline{c_{\mathrm{A}}^0} = c_{\mathrm{A0}}\bar{f}$ and $\overline{c_{\mathrm{B}}^0} = c_{\mathrm{B0}}(1-\bar{f})$.

Given the supersaturation Δc, the expression of nucleation rate R_{N} as a function of the local supersaturation Δc is proposed by Baldyga et al.:[10]

$$R_{\mathrm{N}} = 6.0\times10^{15}(\Delta c)^{1.775}\ \mathrm{no./(m^3\ s)}, \Delta c \le 0.01\ (\mathrm{kmol\ m^{-3}})$$
$$R_{\mathrm{N}} = 2.53\times10^{42}(\Delta c)^{15.0}\ \mathrm{no./(m^3\ s)}, \Delta c > 0.01\ (\mathrm{kmol\ m^{-3}}) \quad (16)$$

Using the beta function $\phi(x,f)$, the local average nucleation rate can be described as

$$\overline{R_{\mathrm{N}}} = \int_0^1 R_{\mathrm{N}}(f)\phi(f)\,\mathrm{d}f \quad (17)$$

The crystal growth rate, G, is described by a two-step diffusion−adsorption model,[21] resulting in the following kinetic rate expression:

$$G = k_{\mathrm{r}}(\sqrt{c_{\mathrm{As}}c_{\mathrm{Bs}}} - \sqrt{K_{\mathrm{sp}}})^{\sigma} = k_{\mathrm{D}}(c_{\mathrm{A}} - c_{\mathrm{As}}) = k_{\mathrm{D}}(c_{\mathrm{B}} - c_{\mathrm{Bs}})\ (\mathrm{m\ s^{-1}}) \quad (18)$$

where c_{is} is the concentration of species i near the crystal surface at the limit of the adsorption layer and the coefficient k_{D} can be calculated from the mass transfer coefficient k_{d}, that is, $k_{\mathrm{D}} = k_{\mathrm{d}}M/\rho$ (assuming that $k_{\mathrm{DA}} = k_{\mathrm{DB}} = k_{\mathrm{D}}$). The measured k_{D} was in the range of $10^{-8}-10^{-7}$ (m s^{-1})(m^3 mol^{-1}).[22] In this work, the value 4×10^{-8} (m s^{-1})(m^3 mol^{-1}) was used. The parameters used in our simulations are listed in Table 1.

Assuming that all moments are proportional to the solid phase concentration,[19] $\overline{G_{mj}}$ in eqs 1 and 2 can be described by using the composition PDF:

$$\overline{Gm_{j-1}} = j\frac{\overline{m_{j-1}}}{\overline{c_{\mathrm{C}}}}\int_0^1 G(x,f)c_{\mathrm{C}}(x,f)\phi(x,f)\,\mathrm{d}f \quad (19)$$

Equation 1 then becomes

$$\frac{\partial(\overline{u_{pi}}\,\overline{m_j})}{\partial x_i} = \frac{\partial}{\partial x_i}\left(D_{\mathrm{PT}}\frac{\partial \overline{m_j}}{\partial x_i}\right) + 0^j\overline{R_N} + j\frac{\overline{m_{j-1}}}{\overline{c_{\mathrm{C}}}}\int_0^1 G(x,f)c_{\mathrm{C}}(x,f)\phi(x,f)\,\mathrm{d}f \quad (20)$$

4. Model Assumption and Simulation Procedure

In setting up the mathematical models, the following assumptions were made:

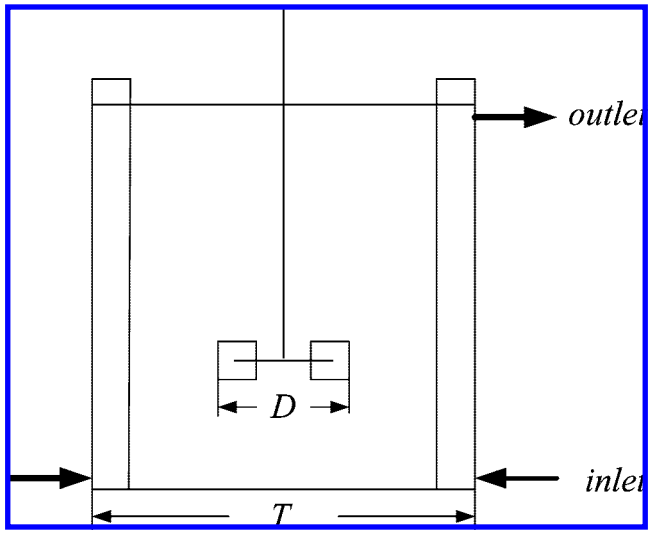

Figure 1. Sketch of the stirred tank.

Table 1. Parameters Used in the Simulations

parameter	value	unit
crystal density, ρ	4480	kg m^{-3}
liquid viscous, μ	10^{-3}	kg m s^{-1}
molecular mass, M_c	233.4	kg kmol^{-1}
solubility product, K_{sp}	1.10×10^{-10}	kmol^2 m^{-6}
surface shape factor, k_a	8.17	
volume shape factor, k_v	1.36	

Table 2. General Variables ϕ, $\Gamma_{\phi eff}$, and Source Terms in Equation 21

φ	$\Gamma_{\varphi eff}$	S_φ
u_r	μ_e	$(1/r)(\partial/\partial r)(\mu_e r(\partial u_r/\partial r)) + (1/r)(\partial/\partial\theta)(\mu_e r(\partial/\partial r)(u_\theta/r)) - 2(\mu_e/r^2)(\partial u_\theta/\partial\theta) - 2(\mu_e u_r/r^2) + (\rho_l u_\theta^2/r) + (\partial/\partial z)(\mu_e \partial u_z/\partial r) - (\partial p/\partial r)\{+\rho_l(\omega^2 r + 2\omega u_\theta)\}$
u_z	μ_e	$(1/r)(\partial/\partial r)(\mu_e r(\partial u_r/\partial z)) + (1/r)(\partial/\partial\theta)(\mu_e(\partial u_\theta/\partial z)) + (\partial/\partial z)(\mu_e(\partial u_z/\partial z)) - (\partial p/\partial z)$
u_θ	μ_e	$\mu_e(\partial/\partial r)(u_\theta/r) - (1/r)(\partial/\partial r)(\mu_e u_\theta) - (\rho_l u_r u_\theta/r) + (\mu_e/r^2)(\partial u_r/\partial\theta) + (1/r)(\partial/\partial r)(\mu_e(\partial u_r/\partial\theta)) + (1/r)(\partial/\partial\theta)(\mu_e r(\partial u_\theta/\partial\theta)) + (1/r)(\partial/\partial\theta)(2\mu_e(u_r/r)) + (\partial/\partial z)(\mu_e r(\partial u_z/\partial\theta)) - (1/r)(\partial p/\partial\theta)\{+\rho_l(-2\omega u_r)\}$
k	μ_e/σ_k	$G - \rho\varepsilon$
ε	μ_e/σ_ε	$\varepsilon/k(C_1 G - C_2\rho\varepsilon)$

(1) The solid phase was assumed to follow the liquid flow because the crystals were very small.

(2) As the solid phase size was less than 10 μm, $D_{PT} = D_T$.

(3) Only the primary nucleation was considered.

(4) The linear crystal growth was independent of crystal size.

(5) Aggregation and breakage as well as the dissolution of particles in a region of undersaturation were neglected.

On the basis of these assumptions, the mixing precipitation can be modeled as follows. The first step was to compute the flow field. The flow turbulence was modeled with a standard $k-\varepsilon$ turbulence model. The velocity components, turbulent kinetic energy k, and viscous dissipation ε under steady state can be calculated by integrating the following equation:[23]

$$\frac{1}{r}\frac{\partial}{\partial r}(\rho r u_r \varphi) + \frac{1}{r}\frac{\partial}{\partial\theta}(\rho u_\theta \varphi) + \frac{\partial}{\partial z}(\rho u_z \varphi) = \frac{1}{r}\frac{\partial}{\partial r}\left(\Gamma_{\varphi eff} r\frac{\partial\varphi}{\partial r}\right) + \frac{1}{r}\frac{\partial}{\partial\theta}\left(\frac{\Gamma_{\varphi eff}}{r}\frac{\partial\varphi}{\partial\theta}\right) + \frac{\partial}{\partial z}\left(\Gamma_{\varphi eff}\frac{\partial\varphi}{\partial z}\right) + S_\varphi \quad (21)$$

The source terms and turbulent diffusivities are presented in Table 2.

The second step was to get the value of $\bar{f}$ by solving eq 5. After that, the variance components σ_1^2, σ_2^2, and σ_3^2 were calculated by solving eqs 6−10, and σ_s^2 resulted. With the distributions of variance components and average mixture fraction, the mixture structure was fully characterized everywhere in the stirred tank. After integrating eqs 2 and 20, the distributions of average concentrations of all species $\bar{c}_i$ and the distributions of the moments $\bar{m}_j$ can be obtained.

Next, the characteristic sizes of the crystal, d_{32}, were computed from the crystal size distribution moments as follows:

$$d_{32} = \frac{\overline{m_3}}{\overline{m_2}} \quad (22)$$

Another parameter characterizing the crystal size distribution, which was used for analysis in this study, was the coefficient of variation (C.V.):

$$\text{C.V.} = \sqrt{\frac{\overline{m_2}\,\overline{m_0}}{\overline{m_1}^2} - 1} \quad (23)$$

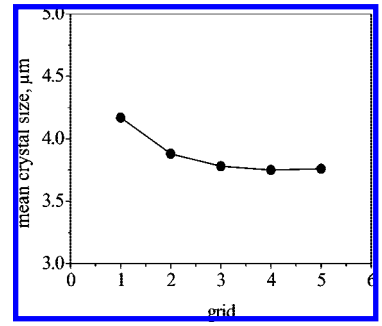

Figure 2. Effect of mesh grid on mean crystal size ($N = 6.2$ rps, $\tau = 57$ s, $c = 0.0095$ kmol/m^3).

5. Computational Grid

Four computational grids of different sizes were used in the simulation to test the effect of the grid independence on the simulated results in this work: 18 × 48 × 24 (grid 1), 24 × 48 × 30 (grid 2), 30 × 72 × 30 (grid 3), 30 × 72 × 40 (grid 4), and 36 × 96 × 60 (grid 5) ($r \times \theta \times z$). The computation was considered converged when the normalized residuals for each primary variable dropped well below 10^{-4}. The crystal mean diameters obtained with different meshes were presented in Figure 2, which shows that the effect of the grids on the simulation procedures was negligible when the grids of 30 × 72 × 30, 30 × 72 × 40, and 36 × 96 × 60 were used. Thus, the grid of 30 × 72 × 40 was used in all subsequent simulations.

6. Results and Discussion

6.1. Flow Field and Distribution of Total Variance. An example map of the mean velocity vector and the distribution of the total variance in the vertical cross-section of the stirred precipitator is presented in Figures 3 and 4, respectively. Vicum and Mazzotti[17] have found that the segregation occurs only in a small region close to feed pipe in a semibatch stirred tank. In Figure 3, it can be noticed that the segregation occurs also in the stirrer region besides the feed position. Because there is a "dead zone" in the stirrer region, reactants cannot be mixed perfectly in this region.

6.2. Effect of Stirrer Speed. Stirrer speed is a major parameter affecting the mixing intensity in a stirred tank. There exist major contradictions in the literature as to the effect of stirred speed on the mean crystal size. An increase in impeller

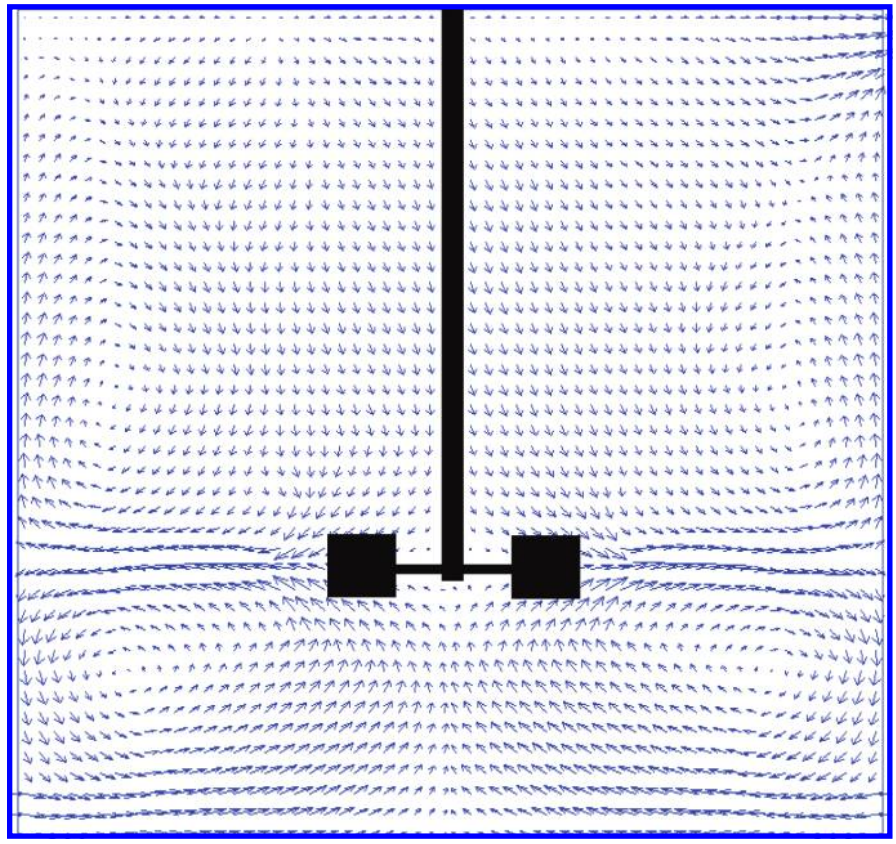

Figure 3. Mean velocity vectors of the stirred tank obtained in the vertical plane between two baffles passing the stirrer shaft ($N = 4.1$ rps, $\tau = 57$ s, $c = 0.038$ kmol/m^3).

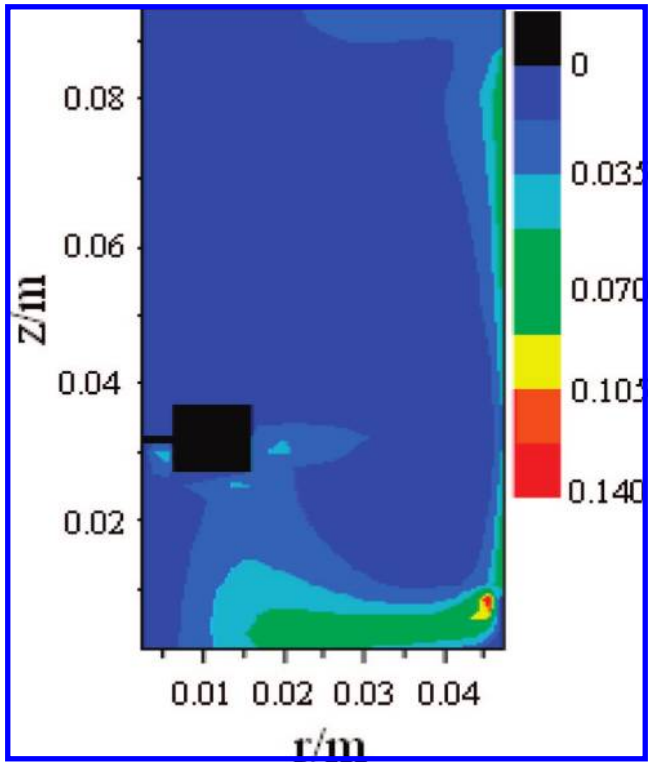

Figure 4. The distribution of total variance σ_s^2 ($N = 4.1$ rps, $\tau = 57$ s, $c = 0.038$ kmol/m^3).

speed was reported to increase, decrease, produce a minimum, or even not affect the mean crystal size. In our work, monotonical increase in the mean crystal size with increasing impeller speed is observed in Figure 5. This may be because the mixing

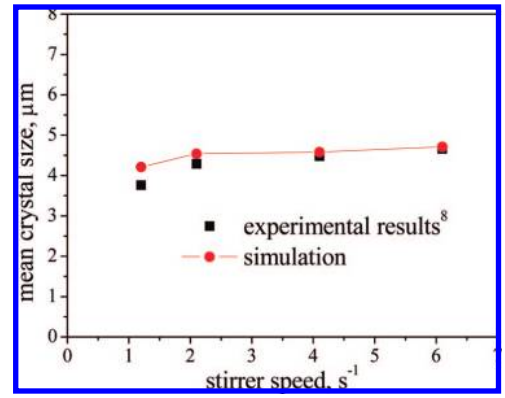

Figure 5. Effect of stirrer speed on mean crystal diameter ($\tau = 57$ s, $c = 0.038$ kmol/m^3).

rate was enhanced with increasing stirrer speed, resulting in the more uniformity of supersaturation and an increase of the crystal growth velocity, which lead to an increase of the mean crystal size finally. Fitchett and Tarbell[2] and van Leeuwen et al.[6] also have found the same trend through experiments. In Figure 5, it can also be seen that there is discrepancy between the experimental results and the simulations at lower stirred speeds, which may be because the flow field cannot be accurately predicted by eq 21 at low Reynolds numbers. The effect of stirrer speed on the coefficient of variation C.V. in Figure 6 seems to be negligible. Baldyga et al.[10] observed that the stirrer speed had no influence on the coefficient of variation C.V. when the reactants were added in a zone of relative low turbulence. The feed positions considered in this work are at the bottom corner and are also in the low turbulence zone, so the coefficient of variation C.V. seemed to be independent of the stirrer speed.

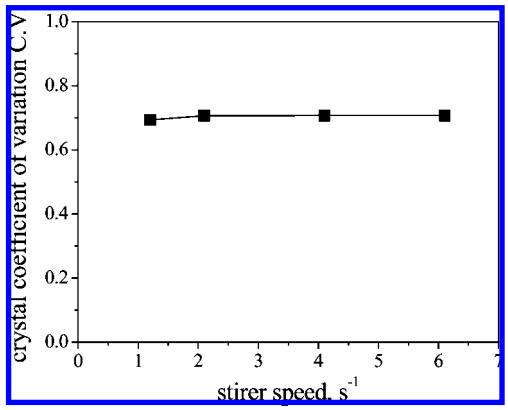

Figure 6. Effect of stirrer speed on the crystal coefficient of variation C.V. (τ = 57 s, c = 0.038 kmol/m^3).

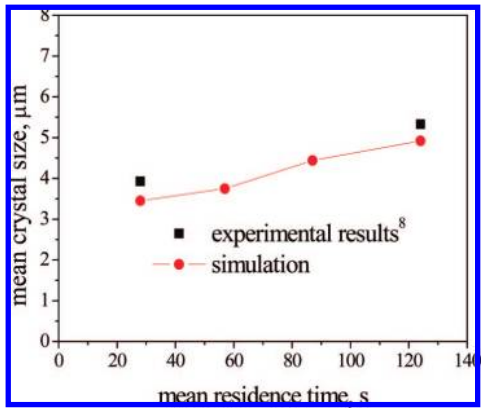

Figure 7. Effect of mean residence time on mean crystal diameter (N = 6.2 rps, c = 0.0095 kmol/m^3).

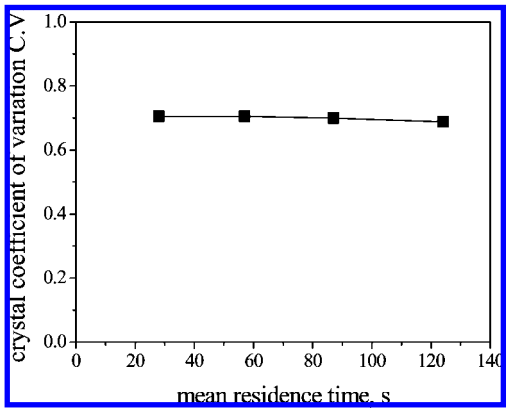

Figure 8. Effect of mean residence time on the crystal coefficient of variation C.V. (N = 6.2 rps, c = 0.0095 kmol/m^3).

6.3. Effect of Mean Residence Time. The residence time is actually the time for the crystal growth in the reactor. The precipitation process with different residence time was numerically predicted in this work. A comparison of the simulation and experimental results for the effect of mean residence time on the mean crystal size is shown in Figure 7. The effect of mean residence time on the coefficient of variation C.V. is shown in Figure 8. Both the predicted and the experimental results in Figure 7 testify an increase of the mean crystal size with increasing the mean residence time. Increasing the mean residence time, the growth time of the crystal increased and resulted in the increase of the mean crystal size. As shown in Figure 7, the simulated values of mean crystal size are underpredicted as compared to the experimental data. Baldyga et al.[19] found that smaller volume shape factor should be used for low feed concentration. The underpredicted results may also be caused by the higher volume shape factor used in this Article when the feed concentration was 0.0095 kmol/m^3. However, with increasing mean residence time, little change of C.V. is seen in Figure 8. Baldyga et al.[10] also found the same results that the mean residence time did not affect the coefficient of variation C.V.

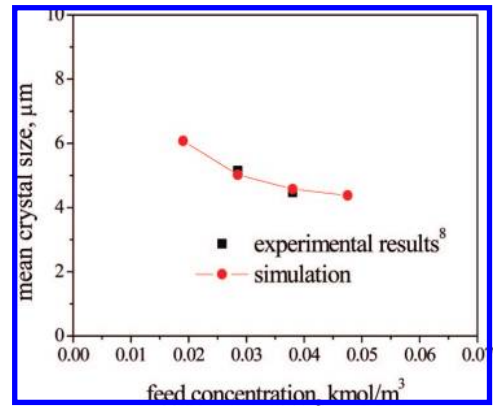

Figure 9. Effect of feed concentration on mean crystal diameter (N = 4.1 rps, τ = 57 s).

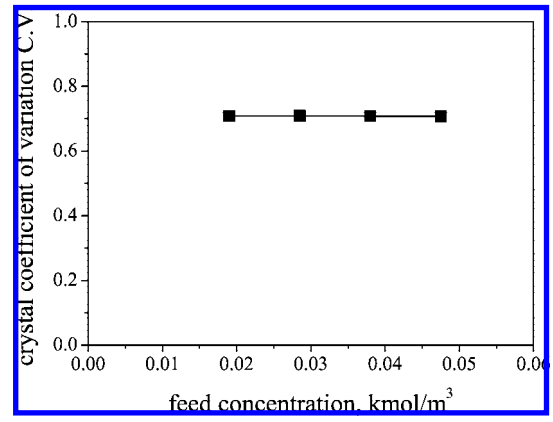

Figure 10. Effect of feed concentration on the crystal coefficient of variation C.V. (N = 4.1 rps, τ = 57 s).

6.4. Effect of Feed Concentration. Figures 9 and 10 show the effect of feed concentration on the mean crystal size and crystal coefficient of variation C.V., respectively. As shown in Figure 9, both the simulation and the experimental data indicate a decrease of the mean crystal size with increasing feed concentration. At low concentration, the increase in the initial concentration of the reactant favors the growth rate more than the nucleation rate. This is evident from the lower exponential power of the heterogeneous nucleation rate (n = 1.775 in eq 16) in comparison to that of the growth rate (r = 4.0). However, for larger initial concentration, the order of nucleation changes from 1.775 to 15.0 in eq 16, the nucleation rate became a very strong function of feed concentration at higher supersaturation values, and thereby smaller particles were produced. However, it can be seen that the crystal coefficient of variation C.V. was almost independent of feed concentration.

7. Conclusion

In this work, the multiple-time-scale turbulent mixer model together with full CFD simulation has been applied to investigate the barium sulfate precipitation process in a continuous stirred tank. The effects of operating conditions such as feed concentra-

tion, stirrer speed, etc. on the precipitation were studied. It is shown that the mean crystal size increased with increasing the stirrer speed and mean residence time. However, when feed concentration was increased, the mean crystal size decreased. The crystal coefficient of variation C.V. was independent of all of the operating conditions considered in this Article. The simulation results were compared to the reported experimental data, and good agreement was observed. It is confirmed that the multiple-time-scale turbulent mixer model considering all scales of mixing can predict correctly the mixing process in a barium sulfate precipitation process in a continuous stirred tank.

Acknowledgment

We acknowledge the National Natural Science Foundation of China (20676134, 20490206, 50574081), 973 Program (2007CB613507, 2004CB217604), and the National Project of Scientific and Technical Supporting Program (2008BAF33D03).

Notation

A, B, C = chemical species
b = width of baffles, m
c_i = concentration of substance i, kmol/m^3
$\overline{c_i}$ = average concentration of substance i, kmol/m^3
c_i^0 = concentration of nonprecipitation tracer, kmol/m^3
$\overline{c_i^0}$ = average concentration of nonprecipitation tracer, kmol/m^3
c_i^∞ = concentration of instantaneous precipitation, kmol/m^3
$\overline{c_i^\infty}$ = average concentration of instantaneous precipitation, kmol/m^3
C.V. = coefficient of variation
d_{32} = mean particle size, μm
D = impeller diameter, m
D_m = molecular diffusivity, m^2/s
D_{PT} = particle turbulent diffusivity, m^2/s
D_T = turbulent diffusivity, m^2/s
E = engulfment parameter, s^{-1}
f = mixture fraction
G = growth rate, m/s
H = height of the tank, m
k = turbulent kinetic energy, m^2/s^2
k_a = surface shape factor
k_v = volume shape factor
$\overline{m_j}$ = mean value of the jth moment of particle number density function
R_{Di} = dissipation rate of variance component, s^{-1}
R_N = nucleation rate, s^{-1}/m^3
$\overline{R_N}$ = average nucleation rate, s^{-1}/m^3
R_{Pi} = production rate of variance component, s^{-1}
T = tank diameter, m
$\overline{u_i}$ = mean velocity vector, m/s
Δc = supersaturation, kmol/m^3
ε = turbulent energy dissipation rate, W/kg
$\Gamma_{\varphi eff}$ = turbulent diffusivity, Pa·s
ρ = density, kg/m^3
σ_s^2,σ_i^2 = variance of mixture fraction
τ = mean residence time, s
$\phi(x,f)$ = probability density function

Literature Cited

(1) Uehare-Nagamine, E.; Armenate, P. M. Effect of process variables on the single-feed semibatch precipitation of barium sulphate. *Trans. Inst. Chem. Eng.* **2001**, *79*, 979–988.

(2) Fitchett, D. E.; Tarbell, J. M. Effect of mixing on the precipitation of barium sulphate in an MSMPR reactor. *AIChE J.* **1990**, *36*, 511–522.

(3) Manth, T.; Mignon, D.; Offermann, H. Experimental investigation of precipitation reactions under homogeneous mixing conditions. *Chem. Eng. Sci.* **1996**, *51*, 2571–2576.

(4) Pohorecki, R.; Baldyga, J. The influence of intensity of mixing on the rate of precipitation. *Proceedings of Industrial Crystallization*; North Holland: Amsterdam, 1979.

(5) Garside, J.; Tavare, N. S. Mixing, reaction and precipitation: limits of micromixing in an MSMPR crystallizer. *Chem. Eng. Sci.* **1985**, *40*, 1485–1493.

(6) Van Leeuwen, M. L. J.; Bruinsma, O. S. L.; Van Rosmalen, G. M. Three-zone approach for precipitation of barium sulphate. *J. Cryst. Growth* **1996**, *166*, 1004–1008.

(7) Pohorecki, R.; Baldyga, J. The use of a new model of micro-mixing for determination of crystal size in precipitation. *Chem. Eng. Sci.* **1985**, *38*, 79–83.

(8) Pohorecki, R.; Baldyga, J. The effects of micromixing and the manner of reactor feeding on precipitation in stirred tank reactors. *Chem. Eng. Sci.* **1988**, *43*, 1949–1954.

(9) Phillips, R.; Rohani, S. Micromixing in a single-feed semi-batch precipitation process. *AIChE J.* **1999**, *45*, 82–92.

(10) Baldyga, J.; Podgorska, W.; Pohorecki, R. Mixing-precipitation model with application to double feed semibatch precipitation. *Chem. Eng. Sci.* **1995**, *50*, 1281–1300.

(11) Garside, J.; Wei, H. Pumped, stirred and maybe precipitated: simulation of precipitation process using CFD. *Acta Polytech. Scand., Chem. Technol. Ser.* **1997**, *244*, 9–15.

(12) Jaworski, Z.; Nienow, A. W. CFD modeling of continuous precipitation of barium sulphate in a stirred tank. *Chem. Eng. J.* **2003**, *91*, 167–174.

(13) Piton, D.; Fox, R. O.; Marcant, B. Simulation of fine particle formation by precipitation using computational fluid dynamics. *Can. J. Chem. Eng.* **2000**, *78*, 983–993.

(14) Marchisio, D. L.; Barresi, A. A.; Fox, R. O. Simulation of turbulent precipitation in a semibatch taylor-couette reactor using CFD. *AIChE J.* **2001**, *47*, 664–676.

(15) Marchisio, D. L.; Fox, R. O.; Barresi, A. A.; Garbero, M.; Baldi, G. On the simulation of turbulent precipitation in a tubular reactor via computational fluid dynamics (CFD). *Trans. Inst. Chem. Eng.* **2001**, *79*, 998–1004.

(16) Wang, Z.; Zhang, Q. H.; Yang, C.; Mao, Z.-S.; Shen, X. Q. Simulation of barium sulfate precipitation using CFD and FM-PDF model in a continuous stirred tank. *Chem. Eng. Technol.* **2007**, *30*, 1642–1649.

(17) Vicum, L.; Mazzotti, M. Multi-scale modeling of a mixing-precipitation process in a semibatch stirred tank. *Chem. Eng. Sci.* **2007**, *62*, 3513–3527.

(18) Baldyga, J.; Orciuch, W. Closure problem for precipitation. *Trans. Inst. Chem. Eng.* **1997**, *75*, 160–170.

(19) Baldyga, J.; Orciuch, W. Barium sulphate precipitation in a pipe-an experimental study and CFD modeling. *Chem. Eng. Sci.* **2001**, *56*, 2435–2444.

(20) Baldyga, J.; Makowski, L.; Orciuch, W. Double-feed semibatch precipitation effects of mixing. *Trans. Inst. Chem. Eng.* **2007**, *85*, 745–752.

(21) Nielsen, A. E. Electrolyte crystal growth mechanisms. *J. Cryst. Growth* **1984**, *67*, 289–310.

(22) Nagata, S.; Nishikawa, M. Mass transfer from suspended micro-particles in agitated liquids. *Proc. First Pacific Chem. Eng. Congress* **1972**, 301–320.

(23) Wang, Z.; Mao, Z.-S.; Yang, C.; Shen, X. Q. CFD approach to the effect of mixing and draft tube on the precipitation of barium sulfate in a continuous stirred tank. *Chin. J. Chem. Eng.* **2006**, *14*, 713–722.

Received for review May 4, 2008
Revised manuscript received September 20, 2008
Accepted October 16, 2008

IE800722F